ACS APPLIED MATERIALS & INTERFACES

Research Article

www.acsami.org

Micro-/Nanostructured Co_3O_4 Anode with Enhanced Rate Capability for Lithium-Ion Batteries

Guoyong Huang,[†] Shengming Xu,*[,†,‡] Shasha Lu,[†] Linyan Li,[†] and Hongyu Sun[§]

[†]Institute of Nuclear and New Energy Technology, Tsinghua University, Beijing 100084, China

[‡]Beijing Key Lab of Fine Ceramics, Tsinghua University, Beijing 100084, China

[§]Beijing National Center for Electron Microscopy, School of Materials Science and Engineering, Tsinghua University, Beijing 100084, China

Supporting Information

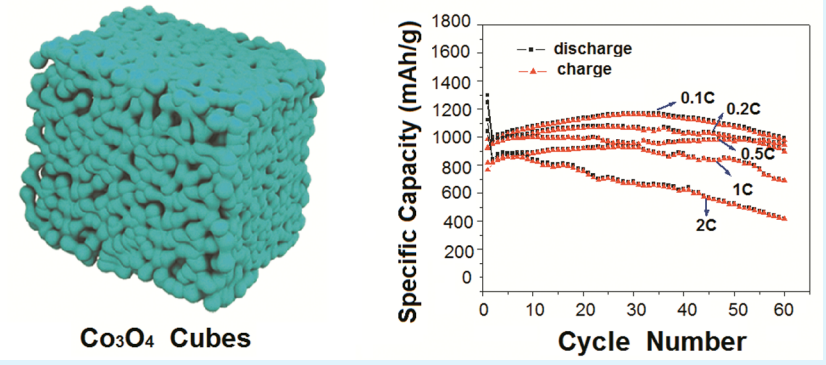

ABSTRACT: Through a facile hydrothermal method with a special surfactant triethanolamine (TEA) followed by thermal treatment, monodispersed micro-/nanostructured Co_3O_4 powders with unique morphology (cube) have been synthesized successfully as anode material for Li-ion batteries (LIBs). The regular Co_3O_4 microcubes (~2.37 μm in the average side length) consist of many irregular nanoparticles (20−200 nm in diameter, 30−40 nm in thickness) bonded to each other, which greatly inherit the morphology and size of the precursor $CoCO_3$. The specific surface area of Co_3O_4 powders is about 5.10 $m^2 \cdot g^{-1}$ by the Brunauer−Emmett−Teller (BET) method, and the average pore size is about 3.08 nm by the Barrett−Joyner−Halenda (BJH) method. In addition, the precursor is verified as a single-crystal, while the mesoporous cubic Co_3O_4 is a polycrystalline characteristic assembled by numerous single-crystal nanoparticles. More remarkable, the high performance of the micro-/nanostructured cubic Co_3O_4 powders has been obtained by the electrochemical measurements including high initial discharge capacities (1298 $mAhg^{-1}$ at 0.1 C and 1041 $mAhg^{-1}$ at 1 C), impressive rate capability, and excellent capacity retention (99.3%, 97.5%, 99.2%, and 89.9% of the first charge capacities after 60 cycles at 0.1 C, 0.2 C, 0.5 C, and 1 C, respectively).

KEYWORDS: *cobalt oxide, micro-/nanostructured, mesoporous, cube, enhanced rate capability, lithium-ion batteries*

INTRODUCTION

High performance Li-ion batteries (LIBs) for application in electric vehicles (EVs) and hybrid electric vehicles (HEVs) require the development of new electrode materials with good cycling stability, high energy density, and rapid-rate capability.[1,2] Transition metal oxides[3,4] (Co_3O_4,[5] CoO,[6] Fe_3O_4,[7] Fe_2O_3,[8] NiO,[9] MnO,[10] CuO,[11] Cu_2O,[12] et al.) are accounted as promising anode materials for these LIBs owing to the higher theoretical capacities (>600 $mAhg^{-1}$) than commercial graphite (<372 $mAhg^{-1}$). Among them, Co_3O_4, which can store eight lithium atoms per formula unit and possess almost the highest reversible capacity (~890 $mAhg^{-1}$), has been extensively investigated for many years.[13−15] Nevertheless, its capacity retention is barely satisfactory due to its large volume expansion upon insertion of lithium-ions and poor electrical conductivity.[16] With the purpose of improving the cycling stability, many researchers have focused on studying nanostructures such as nanospheres,[17] nanowires,[18] nanoplatelets,[19] nanorods,[20] nanosheets,[21,22] nanocages,[23] nanotubes,[24] nanocubes,[25,26] and some other more complex ones.[27,28] The results indicated that the initial charge capacities increased obviously (mostly between 800 $mAhg^{-1}$ and 1000 $mAhg^{-1}$), and the capacity retention ratios were improved (>85% after 40 or 50 cycles) at low rates such as 0.1 and 0.2 C. Basically, three superiorities of the nanostructured materials are here as follows: (1) the huge surface area increases the area of interface and the number of reaction sites between electrolyte and active materials; (2) compared to normal sized particles, the nanoscale components can make diffusion lengths to be shorter and lithium-ions to diffuse much easier; (3) along with lithium-ions inserting and

Received: January 21, 2014
Accepted: May 2, 2014
Published: May 2, 2014

Scheme 1. Preparation Process and Possible Growth Mechanism of Mesoporous Co_3O_4 Cubes with Micro-/Nanoscale Structures

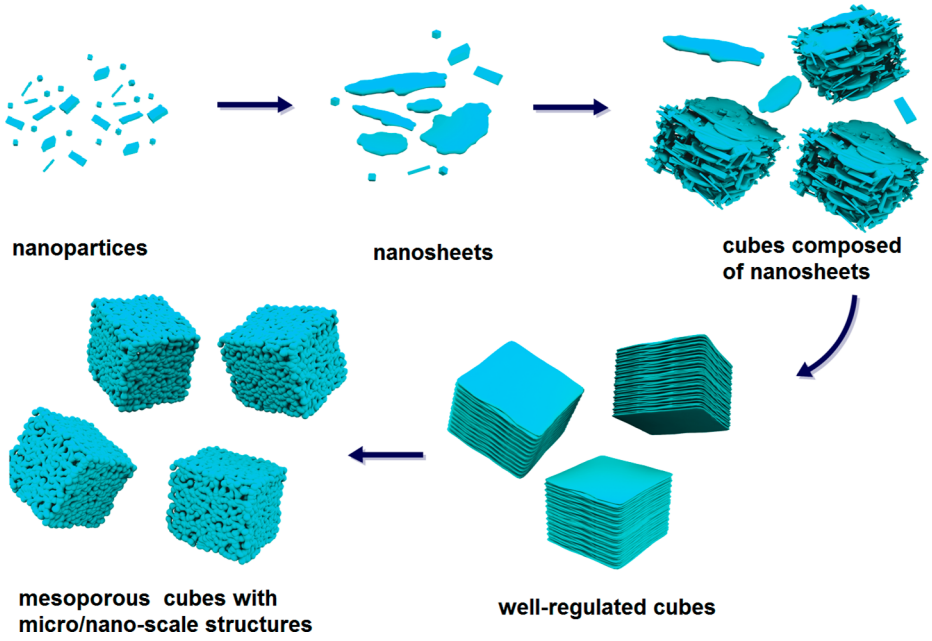

extracting, the big interior space among nanoparticles can accommodate the volume expansion much better.[29] However, the data at high rates such as 1 and 2 C with long cycles (>30 cycles) were very rare in the literature. In other words, the cycling stability of nanostructured Co_3O_4 may be still imperfect at fast discharge and charge process. Some new problems would be brought at the moment: (1) the nanoscale ingredients perhaps agglomerate and fuse easily due to the excessive surface energy; (2) it is easy to increase side reactions and byproducts with too many reaction sites.[30] Therefore, researchers had to mix Co_3O_4 with other anode materials such as carbon,[16,31] carbon nanotubes,[32] and graphene[26,33] to enhance its rate capability; and it is still a great challenge to synthesize a single Co_3O_4 anode with high reversible capacity, excellent rate capability, and improved capacity retention simultaneously.

On the other hand, micro-/nanostructured materials, which are constituted to microscale particles by nanoscale components orderly, can both inherit the advantages of nanomaterials and avoid all of their above shortcomings due to the synergetic effect of integral microstructures, short diffusion lengths among the nanoblocks, and enough small openings to buffer the volume variation.[34−37] SnO_2/C double-shelled hollow spheres have been synthesized by Lou et al.[38] The special spheres possess good cycling stability (73% of the initial charge capacity after more than 100 cycles at 0.8 C), and $CoMn_2O_4$ spinel hierarchical microspheres (4−6 μm in diameter) consisting of many porous nanosheets (~350 nm in thickness) have achieved enhanced rate capability (894 $mAhg^{-1}$, 94.9% of the second discharge capacity after 65 cycles at 100 mAg^{-1}).[39] In addition, multishelled Co_3O_4 hollow microspheres have been prepared with a good cycle ability (*e.g.* the discharge capacity of the quadruple-shelled one remained as high as 1011.5 mAg^{-1} after 30 cycles at 50 mAg^{-1}).[40] However, it is a pity that its electrochemical performance was still not tested at high rates or large current densities with long cycles.

Herein, we have successfully synthesized unique micro-/nanostructured Co_3O_4 through a facile hydrothermal method followed by thermal treatment as anode material for LIBs. The Co_3O_4 powders inherit the special morphology of precursor $CoCO_3$ and obtain mesoporous structure after heat treatment. After being evaluated, the superior electrochemical performance with impressive rate capability and excellent capacity retention is proved as expected.

EXPERIMENTAL SECTION

Materials. All reagents are the analytical grade without further purification. The $Co(CH_3COO)_2{\cdot}4H_2O$ (molecular weight 249.10) and $CO(NH_2)_2$ (molecular weight 60.06) were used as source materials, and the triethanolamine (TEA) ($(HOCH_2CH_2)_3N$, molecular weight 149.19) was used as surfactant.

Synthesis of $CoCO_3$ Cubes. As a typical synthesis, cobaltous acetate (2.50 g), carbamide (3.00 g), and TEA (2.00 g) were dissolved in deionized water step-by-step under vigorous stirring to obtain 100 mL of transparent solution. Then, it was transferred into a Teflon-lined stainless steel autoclave (140 mL), and a thermal treatment was performed for the sealed autoclave in an electric oven at 160 °C for 6 h. After the reaction was over and the autoclave was cooled naturally, the pink powders in the autoclave were collected and washed by centrifugation for three cycles using deionized water and three cycles using pure ethanol. At last, they were dried in a vacuum oven at 60 °C for 24 h.

Synthesis of Mesoporous Co_3O_4 Cubes. In the event of the conversion from the precursor to mesoporous Co_3O_4 cubes, another thermal treatment was performed in air at 600 °C for 10 h with a heating ramp of 10 °C·min^{-1}. Then, the black powders were collected and attired by hand.

Characterization of the Samples. The crystal phases of samples were characterized by X-ray powder diffraction (XRD) (Rigaku, D/Max-2000) using Cu$K\alpha$ radiation with a graphite monochromator at a scanning rate of 1°·min^{-1} with 2theta in the range of 10°−80°. The particle sizes and distributions were analyzed by the laser particle size analyzer (Malvern 2000, measurement range: 0.01−1000 μm). The surface area and pore size were calculated by the Brunauer−Emmett−Teller (BET) method and the Barrett−Joyner−Halenda (BJH) method using the specific surface area and porosity analyzer (Quantachrome, NOVA 3200e). The micromorphologies and others were observed by scanning electron microscope (SEM) (JEOL, JSM 6301, and JSM 5500) and transmission electron microscope (TEM) (JEOL, JSM 2100, and FEI, Tecnai G2 F20).

dx.doi.org/10.1021/am500452t | ACS Appl. Mater. Interfaces 2014, 6, 7236−7243

Electrochemical Characterization. The electrochemical performance of mesoporous Co_3O_4 microcubes as electrode materials were evaluated using coin cells with lithium metal as the reference electrodes. The working electrode was composed of Co_3O_4, acetylene black (ATB), and polytetrafluoroethylene (PTFE) with a weight ratio of Co_3O_4/ATB/PTFE = 7:2:1. The electrolyte solution is 1 mol·L^{-1} $LiPF_6$ dissolved in a mixture of ethylene carbonate (EC), propylene carbonate (PC), and diethyl carbonate (DEC) with a volume ratio of EC/PC/DEC = 3:1:1. The electrode capacity was measured by the galvanostatic discharge−charge method at about 25 °C on the electrochemical test instruments (Land, CT2001A). The cyclic voltammogram (CV) was performed at a scan rate of 0.2 mV·s^{-1} in the range of 0.01−3.00 V (vs Li^+/Li), and the electrochemical impedance spectroscopy (EIS) was obtained over a frequency range from 1 MHz to 0.01 Hz at AC voltage of 10 mV amplitude by Electrochemical workstation (Princeton, Parstat2273).

RESULTS AND DISCUSSION

Scheme 1 illustrates the preparation process and possible growth mechanism of mesoporous Co_3O_4 cubes with micro-/nanoscale structures. Typically, this process includes two steps. (1) Regular $CoCO_3$ microcubes are prepared with the influence of $CO(NH_2)_2$ and TEA. Under the hydrothermal condition, $CO(NH_2)_2$ molecules can hydrolyze homogeneously, and CO_3^{2-} anions are released slowly; $CoCO_3$ molecules are generated through the precipitation reaction of Co^{2+} and CO_3^{2-} with prolonging the reaction time. At first, a lot of irregular particles as crystal nucleuses are formed at 1 h (Figure S1a, Supporting Information). Second, the particles are induced to grow to sheets at 2 h (Figure S1b, Supporting Information), owing to the intrinsic lamellar structures of hexagonal $CoCO_3$. Its (100) and (010) facets possess higher chemical potential than the other facets, and the crystal growth along the [100] and [010] directions can be much easier to release more energy.[41] Then, the primary cubes are formed through the self-assembly aggregation of sheets to reduce the interfacial energy at 3 h (Figure S1c, Supporting Information).[41,42] Finally, due to the impact of the weak alkaline surfactant TEA, which has a favorable interaction with the cobalt ions and coats the $CoCO_3$ particles well, the cubes continue to grow up to the well-defined microcubes without aggregation at 4 h (Figure S1d, Supporting Information). (2) After calcinated under 600 °C for 10 h, the cubic $CoCO_3$ easily turns to mesoporous micro-/nanostructured Co_3O_4 owing to the decomposition reaction and the release of gas CO_2.[14,43,44]

The X-ray powder diffraction (XRD) pattern of the as-prepared precursor is shown in Figure 1. The diffraction peaks are indexed as a pure hexagonal phase of $CoCO_3$, which match well with the standard pattern (JCPDS no. 78-0209, space group R3*c*, $a = b = 4.661$ Å, and $c = 14.961$ Å). The $CoCO_3$ powders show a narrow size distribution (more than 90% in the range of 1.00−3.30 μm), and the final average grain diameter is about 2.37 (Figure 2). The specific surface area is about 0.81 $m^2 \cdot g^{-1}$ calculated based on the nitrogen adsorption isotherm measurement data (Figure S2, Supporting Information) by the Brunauer−Emmett−Teller (BET) method. Meanwhile, the scanning electron microscope (SEM) and transmission electron microscope (TEM) images are shown in Figure 3. The morphology of the corresponding sample is a regular monodispersed cubic shape (Figure 3a and Figure 3b) with an edge length of about 1.00−3.00 μm, which is in accordance with the above results obtained by the laser particle size analyzer. Interestingly, the $CoCO_3$ microcubes have very smooth and dense surface (Figure 3c), and each of the

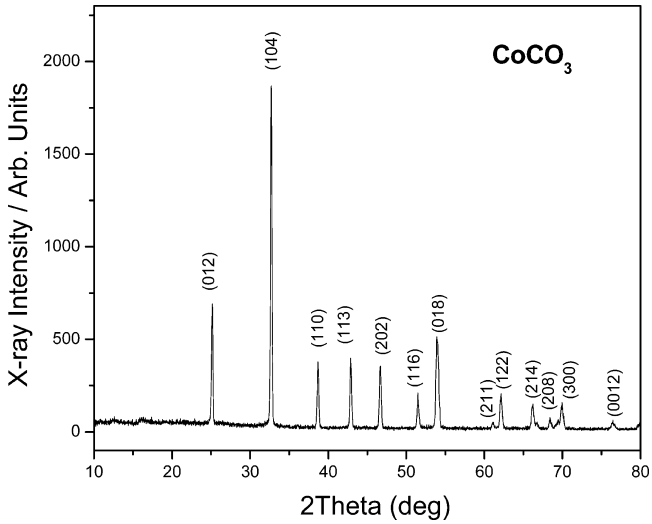

Figure 1. XRD pattern of $CoCO_3$ powders.

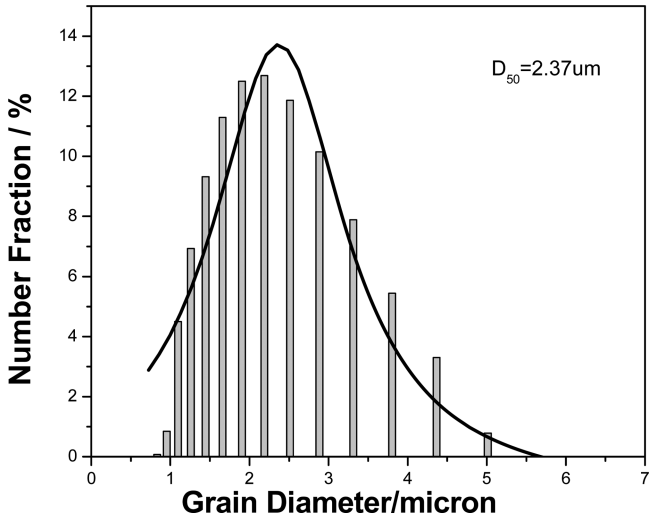

Figure 2. Size distribution of $CoCO_3$ powders.

microcubes is clearly composed of numerous superposed nanosheets (30−40 nm in thickness, measured from Figure 3d). What is more, the single $CoCO_3$ microcube shows the characteristic of a large degree of single-crystal shown, which is evidenced by the selected area electron diffraction (SAED) pattern with clear diffraction spots (Figure 3f, from circled area in Figure 3e).

The XRD pattern of the calcined product is shown in Figure 4. The diffraction peaks also match well with the standard pattern of cubic phase Co_3O_4 (JCPDS no. 42-1467, space group *Fd*3*m*, $a = b = c = 8.084$ Å), and no diffraction peaks of other impurities are obtained. Meanwhile, the specific surface area is calculated to be about 5.10 $m^2 \cdot g^{-1}$ from the data obtained by BET nitrogen adsorption isotherm measurement (Figure S3, Supporting Information), which is about 6 times larger than the precursor owing to the new multiholes structure. It is shown that the corresponding sample is also a regular cubic shape with a mesoporous structure, greatly inheriting the morphology and size of the precursor by the low-magnification SEM images (Figure 5a and Figure 5b). Furthermore, in the high-magnification SEM images with different angles as Figure 5c and Figure 5d (the sample platform was rotated 45°), it is

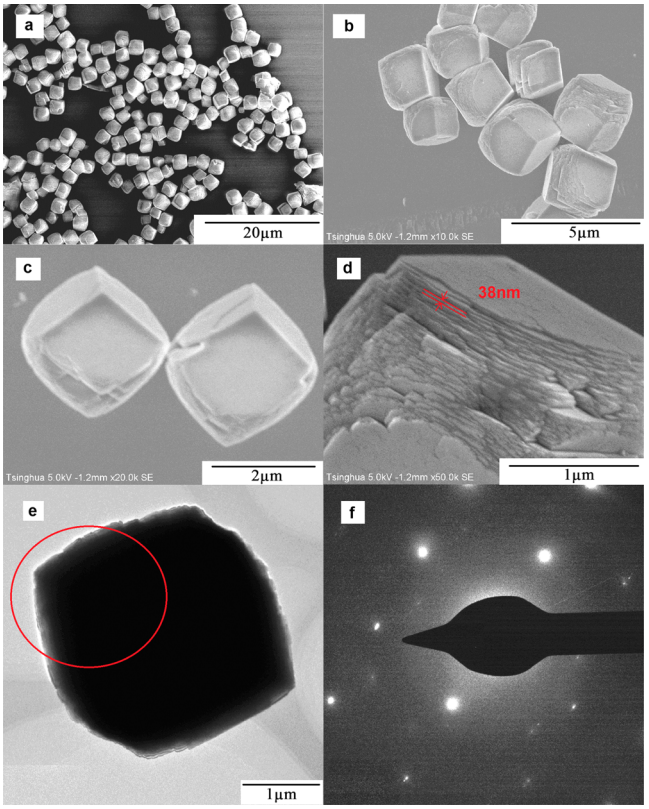

Figure 3. SEM images of $CoCO_3$ powders at magnifications of (a) 2 000, (b) 10 000, (c) 20 000, and (d) 50 000. (e) TEM image of $CoCO_3$ powders. (f) SEAD pattern of $CoCO_3$ powders.

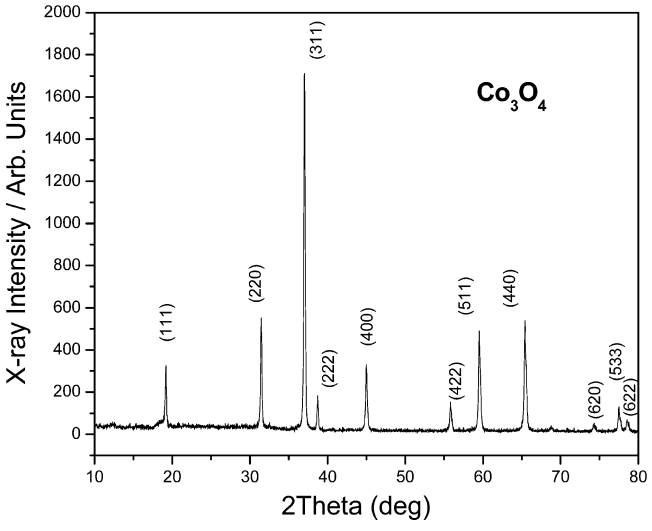

Figure 4. XRD pattern of Co_3O_4 powders.

evident that the single Co_3O_4 microcube is assembled by irregular nanoparticles bonded to each other with the diameter range of 20−200 nm and the thickness form 30 to 40 nm by measuring from its frontage and profile. At the same time, lots of irregular pores can be clearly observed among the nanoparticles, and the average pore size of 3.08 nm and narrow size distribution (more than 90% in the range of 3.00−10.00 nm) were calculated by the Barrett−Joyner−Halenda (BJH) method (Figure S4, Supporting Information). The TEM image in Figure 6a clearly indicates that the mesoporous Co_3O_4 microcube consists of irregular nanoparticles again, and it is a

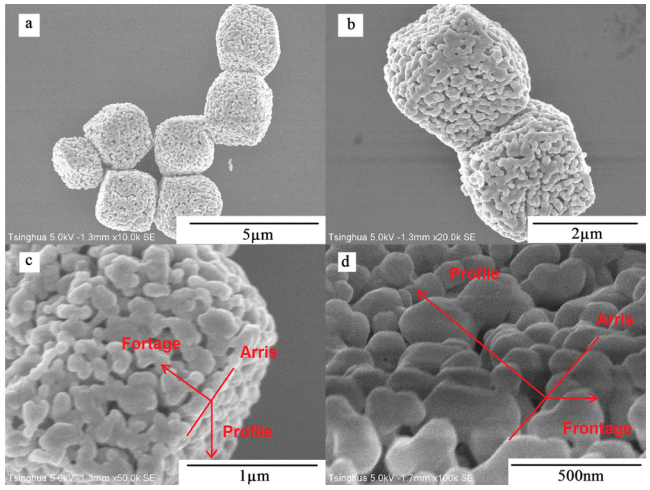

Figure 5. SEM images of Co_3O_4 powders at magnifications of (a) 10 000, (b) 20 000, (c) 50 000, and (d) 100 000.

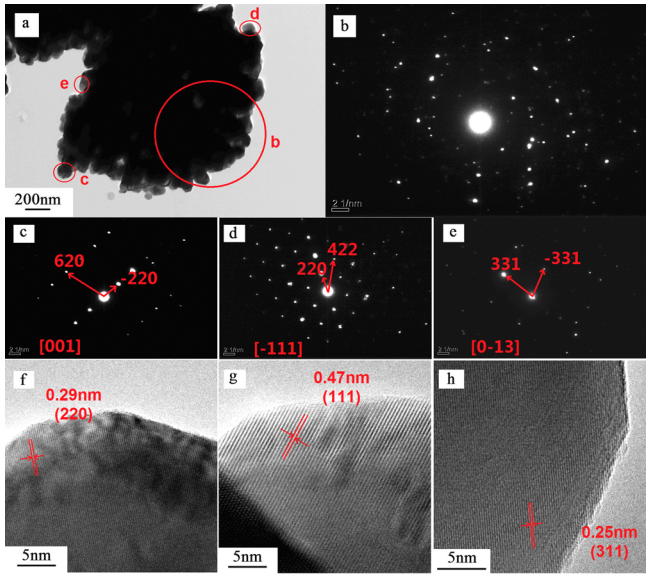

Figure 6. (a) TEM image of Co_3O_4 powders. (b), (c), (d), and (e) SEAD patterns form the corresponding area of (a). (f), (g), and (h) HRTEM images from different positions of (a).

polycrystalline phase shown by the SAED pattern with clear irregular diffraction spots (Figure 6b, from circled area-b in Figure 6a). However, the nanoparticles are different single-crystal characteristics shown in Figure 6c, Figure 6d, and Figure 6e from the corresponding area in Figure 6a, and these SAED patterns can be indexed to [001], [−111], and [0−13] zone axes. In addition, the lattice fringes with lattice spacings of 0.29 nm, 0.47 nm, and 0.25 nm match well with (220), (111), and (311) planes of cubic phase Co_3O_4 shown by the high-resolution transmission electron microscope (HRTEM) images (Figure 6f, Figure 6g, and Figure 6h). In a word, the mesoporous Co_3O_4 microcube with a polycrystalline phase perhaps consists of numerous nanoparticles with single-crystalline nature.

The special structure endows the Co_3O_4 electrodes with excellent performance evaluated by various electrochemical tests. The first five cyclic voltammograms (CV) were investigated at the scanning rate of 0.2 $mV \cdot s^{-1}$ over the voltage range of 0.01−3.00 V (vs Li^+/Li) (Figure 7). At the first cycle,

dx.doi.org/10.1021/am500452t | ACS Appl. Mater. Interfaces 2014, 6, 7236−7243

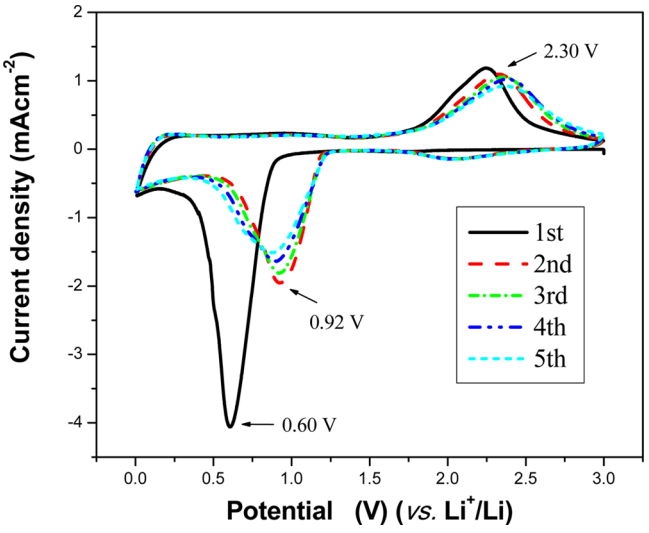

Figure 7. First five cyclic voltammogram curves of Co_3O_4 electrode at a scan rate of 0.2 mV·s^{-1} in the range of 0.01−3.00 V.

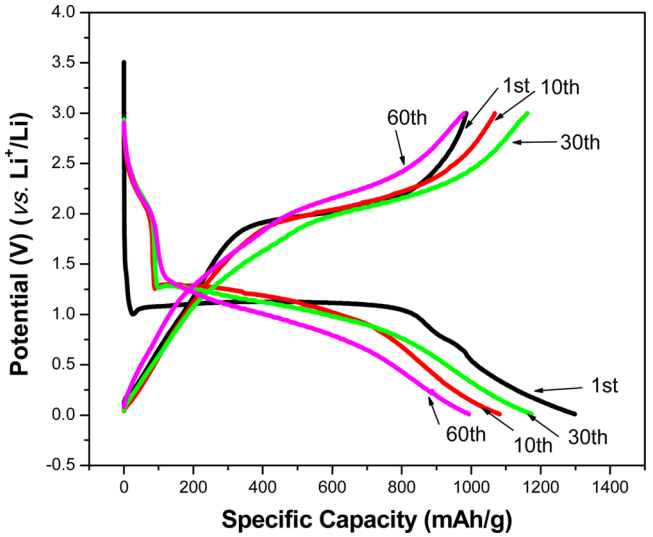

Figure 8. Discharge and charge profiles of Co_3O_4 electrode in the range of 0.01−3.00 V at the rate of 0.1 C.

only a well-defined reduction peak is observed at about 0.60 V, which may be caused by the initial irreversible reduction reaction of Co_3O_4 to Co [eq 1];[27,36] and an obvious anodic peak is recorded at about 2.24 V, which could arise from the oxidation reaction of Co to CoO [eq 2].[27,45] In the subsequent cycles, the reduction peaks are shifted to 0.86−0.92 V, which corresponds to the other reduction reaction of CoO to Co [eq 3],[27,36,45] but the oxidation peaks are observed at 2.24−2.36 V with a little change corresponding to the same oxidation reaction [eq 2]. It indicates that the electrochemical reaction is excellent reversible after the first cycle. In addition, the intensity of reduction peaks decreases after the second cycle due to the formation of the irreversible solid electrolyte interface (SEI) film and the irreversible reduction reaction.[45]

$$Co_3O_4 + 8Li^+ + 8e^- \rightarrow 3Co + 4Li_2O \quad (1)$$

$$Co + Li_2O \rightarrow CoO + 2Li^+ + 2e^- \quad (2)$$

$$CoO + 2Li^+ + 2e^- \rightarrow Co + Li_2O \quad (3)$$

The discharge and charge profiles of the micro-/nano-structured Co_3O_4 anode in the voltage range from 0.01 to 3.00 V (vs Li^+/Li) at 0.1 C are shown in Figure 8. Similar to the previous report,[46] in the first discharge curve, the potential value quickly falls to the plateau (∼1.00 V), which may be ascribed to the conversion from Co_3O_4 to Co; and then gradually declines to the cutoff voltage (0.01 V), which should be associated with the formation of a polymer/gel-like film on the surface of Co_3O_4 particles.[29,45,47] It is shown that the initial discharge and charge capacities are 1298 mAhg^{-1} and 986 mAhg^{-1}, respectively, and the irreversible capacity loss may arise from the formation of the SEI film (irreversible reactions) during the first discharge cycle.[47,48] The following discharge/charge curves tend to be stable, the 10th and 30th cycle processes exhibit similar electrochemical behavior with an approximate charge capacity between 1060 mAhg^{-1} and 1173 mAhg^{-1}, and then the 60th charge capacity slowly decreases to 980 mAhg^{-1}. All of the capacities as above are larger than its theoretical total capacity (890 mAhg^{-1}), that it is probably caused by the reversible formation/dissolution of the polymer/gel-like film contributing to an additional reversible capacity besides the electrochemical conversion reaction between cobalt oxide and Co.[17,29,47]

Figure 9 represents the systematic cycling performance of mesoporous Co_3O_4 microcubes at different rates of 0.1 C, 0.2

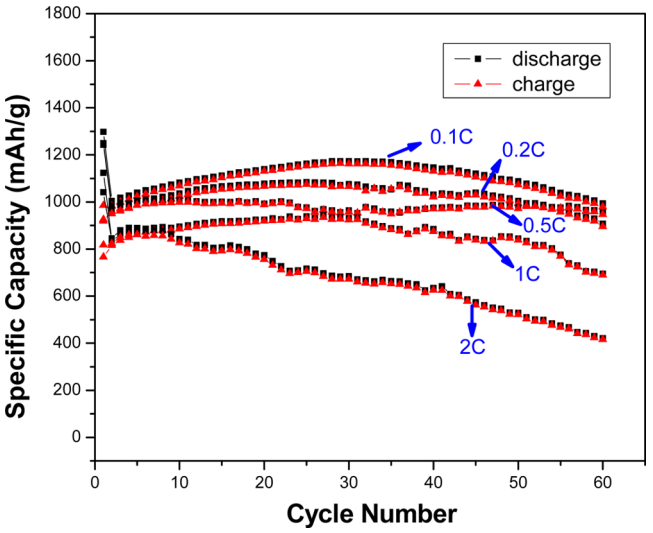

Figure 9. Cycling performances of Co_3O_4 electrodes at different rates of 0.1 C, 0.2 C, 0.5 C, 1 C, and 2 C.

C, 0.5 C, 1 C, and 2 C (1 C = 890 mAg^{-1}). It is shown that the change trends of capacity versus cycle number under low rates (0.1 C, 0.2 C, and 0.5 C) are very similar. (1) The capacities nearly keep constant even after 60 cycles, and the charge capacity retention ratios are 99.3%, 97.5%, and 99.2%, respectively. (2) More interesting, the capacities of the previous cycles from the second cycle increase slowly and gradually. The maximum discharge capacities could reach up to 1173 mAhg^{-1}, 1075 mAhg^{-1}, and 997 mAhg^{-1}, respectively. It is likely that Li-ion diffusion is activated and stabilized gradually during cycling.[15] (3) The Coulombic efficiency of every cycle except the first one is more than 98%. When the rates increase to 1 and 2 C, the initial discharge capacities still keep high values (1041 mAhg^{-1} and 1023 mAhg^{-1}); after 60 cycles, the charge capacities fall slowly to 689 mAhg^{-1} and 416 mAhg^{-1}, which

dx.doi.org/10.1021/am500452t | ACS Appl. Mater. Interfaces 2014, 6, 7236−7243

still mark about 89.9% and 50.8% of the first charge capacities. Through the above tests at high rates with long cycles, the excellent capacity retention of the micro-/nanostructured Co_3O_4 anode is proved. To further investigate the rate capability, one of the most critical issues with the LIBs application, the Co_3O_4 electrode was tested at various constant rates between 0.1 and 10 C shown in Figure 10. The reversible

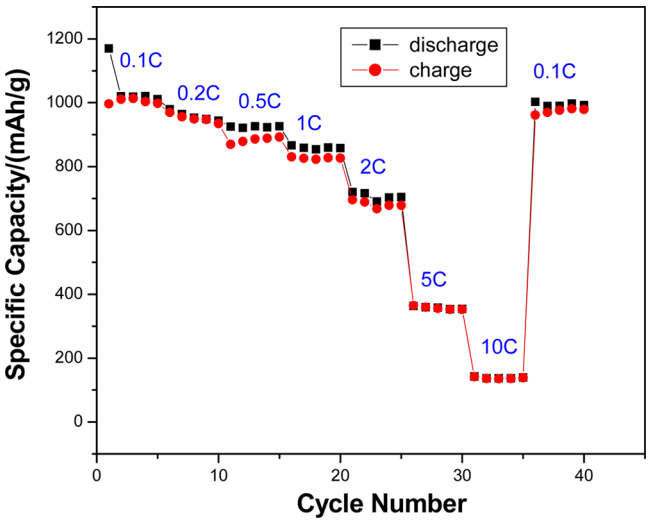

Figure 10. Rate capability of Co_3O_4 electrode at various rates.

capacities are about 1010 $mAhg^{-1}$, 950 $mAhg^{-1}$, 890 $mAhg^{-1}$, 820 $mAhg^{-1}$, 670 $mAhg^{-1}$, 350 $mAhg^{-1}$, and 130 $mAhg^{-1}$ at 0.1 C, 0.2 C, 0.5 C, 1 C, 2 C, 5 C, and 10 C, respectively. Although the material exhibits very low values at large current densities (5 and 10 C), it can regain to deliver a high reversible capacity (980 $mAhg^{-1}$) when the rate turns back to 0.1 C after 35 cycles. Hence, the Co_3O_4 anode with micro-/nanoscale structure illustrates advanced reversible capacity, improved capacity retention, and enhanced rate performance, which has reached the level of the composites (Co_3O_4/graphene and Co_3O_4/carbon nanotubes).[32,33]

To investigate the enhanced electronic conductivity, the electrochemical impedance spectroscopy (EIS) measurements were performed with the frequency range from 1 MHz to 0.01 Hz at the first, fifth, 30th, and 60th cycle at 0.1 C shown in Figure 11. All of the measured values have similar Nyquist plots consisting of a semicircle at high-frequency region, indicating the charge transfer resistance, and an approximate straight line at low-frequency region, representing the lithium-ions diffusion process in electrodes.[48−50] With the increase of the cycle times, the diameter of the semicircle increases longer and longer, which indicates that the charge transfer resistance value of the electrode grows up. The possible reasons may be the decomposition of the electrolyte and decrease of electrical conductivity continually.[39] Remarkably, as shown in Figure 12, the structure of Co_3O_4 microcubes after 60 cycles at 0.1 C has negligible change and displays attractive morphological stability. It is perhaps one of the reasons for the good cycling performance of these materials.

The improved electrochemical performance could be attributed to the unique morphology and special structures of the mesoporous cubic micro-/nanostructured Co_3O_4 powders. (1) The nanoparticles with a thin thickness (30−40 nm) and high specific surface area have all of superiorities as other

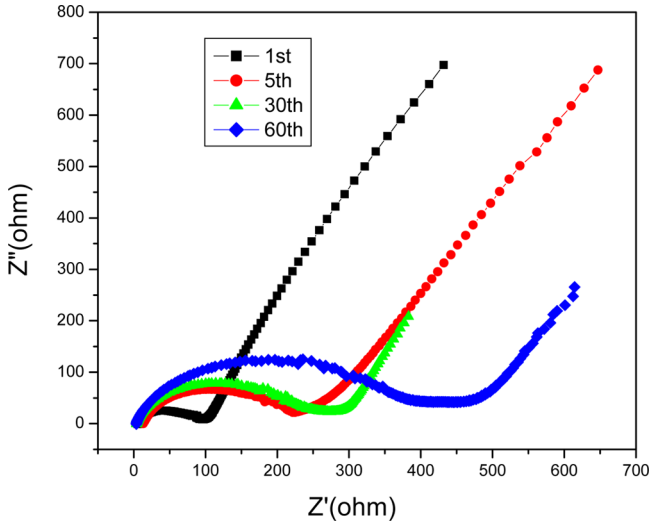

Figure 11. Nyquist plots of the Co_3O_4 electrode after different cycles at 0.1 C measured with an amplitude of 10 mV over the frequency range of 1 MHz and 0.01 Hz.

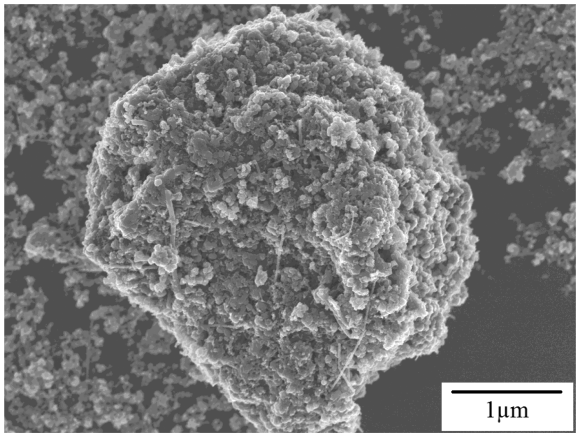

Figure 12. SEM image of the Co_3O_4 electrode (the mixture of Co_3O_4/ATB/PVDF) after 60 cycles at 0.1 C.

nanostructured materials (*e.g.*, shortening the charge transfer pathway, effectively improving the electrical contact and lithium absorption during electrochemical reactions). (2) The regular cubes with a microscale side length (1.00−3.00 μm) consisting of many nanoparticles bonded to each other can prevent them from agglomeration and fragmentation. (3) The mesoporous structure with very small average porous diameter (~3.08 nm) can further enlarge the surface area and promote electrolyte diffusion. (4) The single-crystal structure may be more orderly and definitely increase the efficiency of lithiation and delithiation.

CONCLUSIONS

In summary, mesoporous Co_3O_4 microcubes (~2.37 μm in the average side length) with micro-/nanoscale structures, which are composed of many nanoparticles (20−200 nm in diameter, 30−40 nm in thickness) bonded to each other, have been synthesized as anode material for LIBs.[51] The Co_3O_4 powders inherit the special morphology and size of precursor $CoCO_3$, which have been prepared by the facile hydrothermal method with a special surfactant TEA. The precursor $CoCO_3$ microcube is verified as a single-crystal, while the mesoporous

dx.doi.org/10.1021/am500452t | ACS Appl. Mater. Interfaces 2014, 6, 7236−7243

cubic Co_3O_4 has a polycrystalline characteristic consisting of numerous single-crystal nanoparticles specially. The good performance has been obtained by the electrochemical measurements including high initial discharge capacities (1298 $mAhg^{-1}$ at 0.1 C and 1041 $mAhg^{-1}$ at 1 C), excellent capacity retention (99.3%, 97.5%, and 99.2% of the first charge capacities after 60 cycles at 0.1 C, 0.2 C, and 0.5 C; especially during the high rate of 1 C, 89.9% of the first charge capacity after 60 cycles), and impressive rate capability (980 $mAhg^{-1}$ when the rate turns back to 0.1 C after 35 cycles at different high rates such as 5 and 10 C). Basically, the micro-/nanoscale structures perhaps create a new avenue for the next generation of Co_3O_4 anode with good electrochemical performance.

■ ASSOCIATED CONTENT

Supporting Information

SEM images of $CoCO_3$ with different reaction times. N_2 adsorption isotherms of $CoCO_3$ powders and Co_3O_4 powders. N_2 adsorption/desorption isotherms of Co_3O_4 powders and the inset is the BJH pore-size distribution of the corresponding materials. This material is available free of charge via the Internet at http://pubs.acs.org.

■ AUTHOR INFORMATION

Corresponding Author

*Phone:+86 10 62772055. E-mail: smxu@tsinghua.edu.cn.

Notes

The authors declare no competing financial interest.

■ ACKNOWLEDGMENTS

This work was supported by the National Natural Science Foundation of China (Grant Nos. 51274130 and 51074096).

■ REFERENCES

(1) Dunn, B.; Kamath, H.; Tarascon, J. M. Electrical Energy Storage for the Grid: a Battery of Choices. *Science* **2011**, *334*, 928−935.

(2) Chen, J. J. Recent Progress in Advanced Materials for Lithium Ion Batteries. *Materials* **2013**, *6*, 156−183.

(3) Idota, Y.; Kubota, T.; Matsufuji, A.; Maekawa, Y.; Miyasaka, T. Tin-Based Amorphous Oxide: a High-Capacity Lithium-Ion-Storage Material. *Science* **1997**, *276*, 1395−1397.

(4) Poizot, P.; Laruelle, S.; Grugeon, S.; Dupont, L.; Tarascon, J. M. Nano-Sized Transition-Metal Oxides as Negative-Electrode Materials for Lithium-Ion Batteries. *Nature* **2000**, *407*, 496−499.

(5) Yan, N.; Hu, L.; Li, Y.; Wang, Y.; Zhong, H.; Hu, X. Y.; Kong, X. K.; Chen, Q. W. Co_3O_4 Nanocages for High-Performance Anode Material in Lithium-Ion Batteries. *J. Phys. Chem. C* **2012**, *116*, 7227−7235.

(6) Zhang, M.; Jia, M. Q.; Jin, Y. H.; Shi, X. R. Synthesis and Electrochemical Performance of CoO/Graphene Nanocomposite as Anode for Lithium Ion Batteries. *Appl. Surf. Sci.* **2012**, *263*, 573−578.

(7) Wu, Y.; Wei, Y.; Wang, J. P.; Jiang, K. L.; Fan, S. S. Conformal Fe_3O_4 Sheath on Aligned Carbon Nanotube Scaffolds as High-Performance Anodes for Lithium Ion Batteries. *Nano Lett.* **2013**, *13*, 818−823.

(8) Zhu, X. J.; Zhu, Y. W.; Murali, S.; Stoller, D. M.; Ruoff, S. R. Nanostructured Reduced Graphene Oxide/Fe_2O_3 Composite as a High-Performance Anode Material for Lithium Ion Batteries. *ACS Nano* **2011**, *5*, 3333−3338.

(9) Zhang, G. H.; Chen, Y. J.; Qu, B. H.; Hu, L. L.; Mei, L.; Lei, D. N.; Li, Q.; Chen, L. B.; Li, Q. H.; Wang, T. H. Synthesis of Mesoporous NiO Nanospheres as Anode Materials for Lithium Ion Batteries. *Electrochim. Acta* **2012**, *80*, 140−147.

(10) Zhong, K. F.; Zhang, B.; Luo, S. H.; Wen, W.; Li, H.; Huang, X. J.; Chen, L. Q. Investigation on Porous MnO Microsphere Anode for Lithium Ion Batteries. *J. Power Sources* **2011**, *196*, 6802−6808.

(11) Wang, L. L.; Gong, H. X.; Wang, C. H.; Wang, D.; Tang, K. B.; Qian, Y. T. Facile Synthesis of Novel Tunable Highly Porous CuO Nanorods for High Rate Lithium Battery Anodes with Realized Long Cycle Life and High Reversible Capacity. *Nanoscale* **2012**, *4*, 6850−6855.

(12) Liu, D. Q.; Yang, Z. B.; Wang, P.; Li, F.; Wang, D. S.; He, D. Y. Preparation of 3D Nanoporous Copper-Supported Cuprous Oxide for High-Performance Lithium Ion Battery Anodes. *Nanoscale* **2013**, *5*, 1917−1921.

(13) Du, H. M.; Jiao, L. F.; Wang, Q. H.; Yang, J. Q.; Guo, L. J.; Si, Y. C.; Wang, Y. J.; Yuan, H. T. Facile Carbonaceous Microsphere Templated Synthesis of Co_3O_4 Hollow Spheres and their Electrochemical Performance in Supercapacitors. *Nano Res.* **2013**, *6*, 87−98.

(14) Rui, X. H.; Tan, H. T.; Sim, D. H.; Liu, W. L.; Xu, C.; Hng, H. H.; Yazami, R.; Lim, T. M.; Yan, Q. Y. Template-Free Synthesis of Urchin-like Co_3O_4 Hollow Spheres with Good Lithium Storage Properties. *J. Power Sources* **2013**, *222*, 97−102.

(15) Venugopal, N.; Lee, D. J.; Lee, Y. J.; Sun, Y. K. Self-Assembled Hollow Mesoporous Co_3O_4 Hybrid Architectures: a Facile Synthesis and Application in Li-Ion Batteries. *J. Mater. Chem. A* **2013**, *1*, 13164−13170.

(16) Liu, X. G.; Or, S. W.; Jin, C. G.; Lv, Y. H.; Li, W. H.; Feng, C.; Xiao, F.; Sun, Y. P. Co_3O_4/C Nanocapsules with Onion-like Carbon Shells as Anode Material for Lithium Ion Batteries. *Electrochim. Acta* **2013**, *100*, 140−146.

(17) Sun, Y.; Feng, X. Y.; Chen, C. H. Hollow Co_3O_4 Thin Films as High Performance Anodes for Lithium-Ion Batteries. *J. Power Sources* **2011**, *196*, 784−787.

(18) Nam, K. T.; Kim, D. W.; Yoo, P. J.; Chiang, C. Y.; Meethong, N.; Hammond, P. T.; Chiang, Y. M.; Belcher, A. M. Virus-Enabled Synthesis and Assembly of Nanowires for Lithium Ion Battery Electrodes. *Science* **2006**, *312*, 885−888.

(19) Lu, Y.; Wang, Y.; Zou, Y. Q.; Jiao, Z.; Zhao, B.; He, Y. Q.; Wu, M. H. Macroporous Co_3O_4 Platelets with Excellent Rate Capability as Anodes for Lithium Ion Batteries. *Electrochem. Commun.* **2010**, *12*, 101−105.

(20) Vijayanand, S.; Kannan, R.; Potdar, H. S.; Pillai, V. K.; Joy, P. A. Porous Co_3O_4 Nanorods as Superior Electrode Material for Supercapacitors and Rechargeable Li-Ion Batteries. *J. Appl. Electrochem.* **2013**, *43*, 995−1003.

(21) Pan, L.; Li, L.; Zhu, Q. Y. Facile Synthesis of Co_3O_4 and Ag/Co_3O_4 Nanosheets and their Electrocatalytic Properties. *J. Sol.-Gel. Sci. Technol.* **2013**, *67*, 573−579.

(22) Chen, G.; Fu, E. G.; Zhou, M.; Xu, Y.; Fei, L.; Deng, S. G.; Chaitanya, V.; Wang, Y. Q.; Luo, H. M. A Facile Microwave-Assisted Route to $Co(OH)_2$ and Co_3O_4 Nanosheet for Li-Ion Battery. *J. Alloys Compd.* **2013**, *578*, 349−354.

(23) Liu, D. Q.; Wang, X.; Wang, X. B.; Tian, W.; Bando, Y.; Golberg, D. Co_3O_4 Nanocages with Highly Exposed {110} Facets for High-Performance Lithium Storage. *Sci. Rep.* **2013**, *3*, 2543−2548.

(24) Xu, J.; Gao, L.; Cao, J. Y.; Wang, W. C.; Chen, Z. D. Preparation and Electrochemical Capacitance of Cobalt Oxide (Co_3O_4) Nanotubes as Supercapacitor Material. *Electrochim. Acta* **2010**, *56*, 732−736.

(25) Liu, X. M.; Long, Q.; Jiang, C. H.; Zhan, B. B.; Li, C.; Liu, S. J.; Zhao, Q.; Huang, W.; Dong, X. C. Facile and Green Synthesis of Mesoporous Co_3O_4 Nanocubes and their Applications for Supercapacitors. *Nanoscale* **2013**, *5*, 6525−6529.

(26) Su, L. W.; Zhou, Z.; Qin, X.; Tang, Q. W.; Wu, D. H.; Shen, P. W. $CoCO_3$ Submicrocube/Graphene Composites with High Lithium Storage Capability. *Nano Energy* **2013**, *2*, 276−282.

(27) Xu, M. W.; Wang, F.; Zhao, M. S.; Yang, S.; Song, X. P. Molten Hydroxides Synthesis of Hierarchical Cobalt Oxide Nanostructure and its Application as Anode Material for Lithium Ion Batteries. *Electrochim. Acta* **2011**, *56*, 4876−4881.

(28) Wang, Y.; Xia, H.; Lu, L.; Lin, J. Y. Excellent Performance in Lithium-Ion Battery Anodes: Rational Synthesis of $Co(CO_3)_{0.5}(OH)$-

0.11H_2O Nanobelt Array and its Conversion into Mesoporous and Single-Crystal Co_3O_4. *ACS Nano* **2010**, *4*, 1425−1432.
(29) Wang, F.; Lu, C. C.; Qin, Y. F.; Liang, C. C.; Zhao, M. S.; Yang, S. C.; Sun, Z. B.; Song, X. P. Solid State Coalescence Growth and Electrochemical Performance of Plate-like Co_3O_4 Mesocrystals as Anode Materials for Lithium-Ion Batteries. *J. Power Sources* **2013**, *235*, 67−73.
(30) Rai, A. K.; Gim, J.; Anh, L. T.; Kim, J. Partially Reduced Co_3O_4/Graphene Nanocomposite as an Anode Material for Secondary Lithium Ion Battery. *Electrochim. Acta* **2013**, *100*, 63−71.
(31) Xiong, S. L.; Chen, J. S.; Lou, X. W.; Zeng, H. C. Mesoporous Co_3O_4 and CoO@C Topotactically Transformed from Chrysanthemum-like $Co(CO_3)_{0.5}(OH)\cdot 0.11H_2O$ and their Lithium-Storage Properties. *Adv. Funct. Mater.* **2012**, *22*, 861−871.
(32) He, X. F.; Wu, Y.; Zhao, F.; Wang, J. P.; Jiang, K. L.; Fan, S. S. Enhanced Rate Capabilities of Co_3O_4/Carbon Nanotube Anodes for Lithium Ion Battery Applications. *J. Mater. Chem. A* **2013**, *1*, 11121−11125.
(33) Wu, Z. S.; Ren, W. C.; Wen, L.; Gao, L. B.; Zhao, J. P.; Chen, Z. P.; Zhou, G. M.; Li, F.; Cheng, H. M. Graphene Anchored with Co_3O_4 Nanoparticles as Anode of Lithium Ion Batteries with Enhanced Reversible Capacity and Cyclic Performance. *ACS Nano* **2010**, *4*, 3187−3194.
(34) Lai, X. Y.; Halpert, J. E.; Wang, D. Recent Ddvances in Micro-/Nano-Structured Hollow Spheres for Energy Applications: from Simple to Complex Systems. *Energy Environ. Sci.* **2012**, *5*, 5604−5618.
(35) Wu, X.; Jiang, P.; Cai, W.; Bai, X. D.; Gao, P.; Xie, S. S. Hierarchical ZnO Micro-/Nano-Structure Film. *Adv. Eng. Mater.* **2008**, *10*, 476−481.
(36) Wang, L. M.; Liu, B.; Ran, S. H.; Huang, H. T.; Wang, X. F.; Liang, B.; Chen, D.; Shen, G. Z. Nanorod-Assembled Co_3O_4 Hexapods with Enhanced Electrochemical Performance for Lithium-Ion Batteries. *J. Mater. Chem.* **2012**, *22*, 23541−23546.
(37) Zhang, X. S.; Zhu, F. Y.; Han, M. D.; Sun, X. M.; Peng, X. H.; Zhang, H. X. Self-Cleaning Poly(dimethylsiloxane) Film with Functional Micro/Nano Hierarchical Structures. *Langmuir* **2013**, *29*, 10769−10775.
(38) Lou, X. W.; Li, C. M.; Archer, L. A. Designed Synthesis of Coaxial SnO_2@Carbon Hollow Nanospheres for Highly Reversible Lithium Storage. *Adv. Mater.* **2009**, *21*, 2536−2539.
(39) Hu, L.; Zhong, H.; Zheng, X. R.; Huang, Y. M.; Zhang, P.; Chen, Q. W. $CoMn_2O_4$ Spinel Hierarchical Microspheres Assembled with Porous Nanosheets as Stable Anodes for Lithium-Ion Batteries. *Sci. Rep.* **2012**, *2*, 1−8.
(40) Wang, J. Y.; Yang, N. L.; Tang, H. J.; Dong, Z. H.; Jin, Q.; Yang, M.; Kisailus, D.; Zhao, H. J.; Tang, Z. Y.; Wang, D. Accurate Control of Multishelled Co_3O_4 Hollow Microspheres as High-Performance Anode Materials in Lithium-Ion Batteries. *Angew. Chem.* **2013**, *125*, 1−5.
(41) Cao, F.; Wang, D. Q.; Deng, R. P.; Tang, J. k.; Song, S. Y.; Lei, Y. Q.; Wang, S.; Su, S. Q.; Yang, X. G.; Zhang, H. J. Porous Co_3O_4 Microcubes: Hydrothermal Synthesis, Catalytic and Magnetic Properties. *CrystEngComm* **2011**, *13*, 2123−2129.
(42) Hu, L.; Zhang, P.; Zhong, H.; Zheng, X. R.; Yan, N.; Chen, Q. W. Foamlike Porous Spinel $Mn_xCo_{3-x}O_4$ Material Derived from $Mn_3[Co(CN)_6]_2\cdot nH_2O$ Nanocubes: a Highly Efficient Anode Material for Lithium Batteries. *Chem.—Eur. J.* **2012**, *18*, 15049−15056.
(43) Liu, J.; Xia, H.; Lu, L.; Xue, D. F. Anisotropic Co_3O_4 Porous Nanocapsules Toward High-Capacity Li-Ion Batteries. *J. Mater. Chem.* **2010**, *20*, 1506−1510.
(44) Lou, X. W.; Deng, D.; Lee, J. Y.; Feng, J.; Archer, L. A. Self-Supported Formation of Needlelike Co_3O_4 Nanotubes and their Application as Lithium-Ion Battery Electrodes. *Adv. Mater.* **2008**, *20*, 258−262.
(45) Li, C. C.; Yin, X. M.; Chen, L. B.; Li, Q. H.; Wang, T. H. Synthesis of Cobalt Ion-Based Coordination Polymer Nanowires and their Conversion into Porous Co_3O_4 Nanowires with Good Lithium Storage Properties. *Chem.—Eur. J.* **2010**, *16*, 5215−5221.
(46) Du, H. M.; Jiao, L. F.; Wang, Q. H.; Huan, Q. N.; Guo, L. J.; Si, Y. C.; Wang, Y. J.; Yuan, H. T. Morphology Control of $CoCO_3$ Crystals and their Conversion to Mesoporous Co_3O_4 for Alkaline Rechargeable Batteries Application. *CrystEngComm* **2013**, *15*, 6101−6109.
(47) Lou, X. W.; Jim, D. D.; Lee, Y.; Archer, A. L. Thermal Formation of Mesoporous Single-crystal Co_3O_4 Nano-needles and their Lithium Storage Properties. *J. Mater. Chem.* **2008**, *18*, 4397−4401.
(48) He, C. N.; Wu, S.; Zhao, N. Q.; Shi, C. S.; Liu, E. Z.; Li, J. J. Carbon-Encapsulated Fe_3O_4 Nanoparticles as a High-Rate Lithium Ion Battery Anode Material. *ACS Nano* **2013**, *5*, 4459−4469.
(49) Jia, X. L.; Chen, Z.; Cui, X.; Peng, Y. T.; Wang, X. L.; Wang, G.; Wei, F.; Lu, Y. F. Building Robust Architectures of Carbon and Metal Oxide Nanocrystals toward High-Performance Anodes for Lithium-Ion Batteries. *ACS Nano* **2012**, *6*, 9911−9919.
(50) Prabakar, R. S. J.; Hwang, Y. H.; Bae, E. G.; Shim, S.; Kim, D.; Lah, M. S.; Sohn, K. S.; Pyo, M. SnO_2/Graphene Composites with Self-Assembled Alternating Oxide and Amine Layers for High Li-Storage and Excellent Stability. *Adv. Mater.* **2013**, *25*, 3307−3312.
(51) Hwang, Y. H.; Bae, E. G.; Sohn, K. S.; Shim, S.; Song, X. K.; Lah, M. S.; Pyo, M. SnO_2 Nanoparticles Confined in a Graphene Framework for Advanced Anode Materials. *J. Power Sources* **2013**, *240*, 683−690.